

Impacts of aerosol direct effects on tropospheric ozone through changes in atmospheric dynamics and photolysis rates

Jia Xing¹, Jiandong Wang¹, Rohit Mathur², Shuxiao Wang¹, Golam Sarwar², Jonathan Pleim², Christian
5 Hogrefe², Yuqiang Zhang², Jingkun Jiang¹, David C. Wong², Jiming Hao¹

¹ State Key Joint Laboratory of Environmental Simulation and Pollution Control, School of Environment, Tsinghua University, Beijing 100084, China

²The U.S. Environmental Protection Agency, Research Triangle Park, NC 27711, USA

These authors contributed equally to this work: Jia Xing & Jiandong Wang

10 *Correspondence to: Shuxiao Wang (email: shxwang@tsinghua.edu.cn; phone: +86-10-62771466; fax: +86-10-62773650)

Abstract. Aerosol direct effects (ADE), i.e., scattering and absorption of incoming solar radiation, reduce radiation reaching the ground and the resultant photolysis attenuation can decrease ozone (O₃) formation in polluted areas. One the other hand, evidence also suggests that ADE associated cooling suppresses atmospheric ventilation thereby enhancing surface-level O₃. Assessment of ADE impacts is thus important for understanding emission reduction strategies that seek co-benefits associated with reductions in both particulate matter and O₃ levels. This study quantifies the impacts of ADE on tropospheric ozone by using a two-way online coupled meteorology and atmospheric chemistry model, WRF-CMAQ, instrumented with process analysis methodology. Two manifestations of ADE impacts on O₃ including changes in atmospheric dynamics (Δ Dynamics) and changes in photolysis rates (Δ Photolysis) were assessed separately through multiple scenario simulations for January and July of 2013 over China. Results suggest that ADE reduced surface daily maxima 1h O₃ (DM1O₃) in China by up to 39 $\mu\text{g m}^{-3}$ through the combination of Δ Dynamics and Δ Photolysis in January, but enhanced surface DM1O₃ by up to 4 $\mu\text{g m}^{-3}$ in July. Increased O₃ in July is largely attributed to Δ Dynamics which causes a weaker O₃ sink of dry deposition and a stronger O₃ source of photochemistry due to the stabilization of atmosphere. Meanwhile, surface OH is also enhanced at noon in July, though its daytime average values are reduced in January. An increased OH chain length and a shift towards more VOC-limited condition are found due to ADE in both January and July. This study suggests that reducing ADE may have potential risk of increasing O₃ in winter, but it will benefit the reduction of maxima O₃ in summer.

1. Introduction

Photochemistry in the atmosphere is a well-known source for tropospheric ozone (O₃) (e.g., Haagen-Smit and Fox, 1954) and is determined by ambient levels of O₃ precursors (i.e., NO_x and VOC) and photolysis rates which are largely influenced by meteorological factors such as solar irradiance and temperature. It is well known that aerosols influence radiation through light

scattering and absorption, thereby modulating atmospheric radiation and temperature. These aerosol direct effects (ADE) can then impact thermal and photochemical reactions leading to formation of O₃ (Dickerson et al., 1997). Recent studies suggest that the aerosol induced reduction in solar irradiance leads to lower photolysis rates and less O₃ (e.g., Benas et al., 2007), therefore extensive aerosol reductions, particularly in developing regions such as in East Asia, may pose a potential risk by enhancing O₃ levels (Bian et al., 2007; Anger et al., 2016; Wang et al., 2016). For example, Wang et al (2016) found that because of ADE, the surface 1h maximum ozone (noted as DM1O₃) was reduced by up to 12% in eastern China during the EAST-AIRE campaign, suggesting that benefits of PM_{2.5} reductions may be partially offset by increases in ozone associated with reducing ADE.

Ambient O₃ levels are influenced by several sources and sinks. The modulation of photolysis rates by ADE is only one manifestation of ADE impacts on O₃. In addition, ADE modulate the temperature (e.g., Hansen et al., 1997; Mitchell et al., 1995), atmospheric ventilation (e.g., Jacobson et al., 2007; Mathur et al., 2010), cloud and rainfall (e.g., Albrecht, 1989; Liou and Ou, 1989; Twomey, 1977) which also influence the O₃ concentrations. Therefore, ADE can impact air quality through multiple pathways and process chains (Jacobson, 2002; 2010; Jacobson et al., 2007; Wang et al., 2014; Xing et al., 2015a; Ding et al., 2016). For example, Xing et al (2015a) suggested that the O₃ response to ADE is largely contributed by the increased precursor concentrations which enhance the photochemical reaction, presenting an overall positive response of O₃ to ADE by up to 2-3% in eastern China. Assessment of separate contribution from individual processes is necessary for fully understanding how ADE impact O₃.

In China, atmospheric haze is currently one of the most serious environmental issue of concern. Over the next decade, the national government plans to implement stringent control actions aimed at lowering the PM_{2.5} concentrations (Wang et al., 2017). Speculation on whether such extensive aerosol controls will enhance O₃ and oxidation capacity need to be carefully assessed and quantified. Many studies suggest that aerosols may have substantial impacts on ozone through heterogeneous reactions including hydrolysis of N₂O₅, irreversible absorption of NO₂ and NO₃, as well as the uptake of HO₂ (Tang et al., 2004; Tie et al., 2005; Li et al., 2011; Lou et al., 2014). While our model contains comprehensive treatment of the heterogeneous hydrolysis of N₂O₅ (Davis et al., 2008; Sarwar et al., 2012; Sarwar et al., 2014), we have not quantified its impacts on ozone in this study. However, ADE impacts on ozone have not been well evaluated previously. Accurate assessment of the multiple ADE impacts is a prerequisite for accurate policy decision. The process analysis (PA) methodology is an advanced probing tool that enables quantitative assessment of integrated rates of key processes and reactions simulated in the atmospheric model (Jang et al, 1995; Zhang et al., 2009; Xu et al., 2008; Liu et al., 2010; Xing et al., 2011). In this study, we apply the PA methodology in the two-way coupled meteorology and atmospheric chemistry model, i.e., Weather Research and Forecast (WRF) model coupled with the Community Multiscale Air Quality (CMAQ) model developed by U.S. Environmental Protection Agency (Pleim et al., 2008; Mathur et al., 2010; Wong et al., 2012; Yu et al., 2013; Mathur et al., 2014; Xing et al.,

2015b), to examine the process chain interactions arising from ADE and quantify their impacts on O₃ concentration.

The manuscript is organized as following. A brief description of the model configuration, scenario design and PA method is presented in section 2. The O₃ response to ADE is discussed in section 3.1. PA analyses are discussed in section 3.2-3.3. The summary and conclusion is provided in section 4.

5 2. Method

2.1 Modeling System

The two-way coupled WRF-CMAQ model has been detailed and fully evaluated in our pervious papers (Wang et al., 2014; Xing et al., 2015a, b). The meteorological inputs for WRF simulations were derived from the NCEP FNL (Final) Operational Global Analysis data which has 1 degree spatial and 6-hour temporal resolution. NCEP ADP Operational Global Surface Observations were used for surface reanalysis and four dimensional data assimilation. We have tested and chosen proper strength of nudging coefficients, i.e., 0.00005 sec⁻¹ is used for nudging of both u/v-wind and potential temperature, 0.00001 sec⁻¹ is used for nudging of water vapor mixing ratio, to improve model performance without dampening the effects of radiative feedbacks (Hogrefe et al., 2015; Xing et al., 2015b). In the model version used here, concentrations of gaseous species and primary and secondary aerosols are simulated by using Carbon Bond 05 gas-phase chemistry (Sarwar et al., 2008) and the sixth-generation CMAQ modal aerosol model (AERO6) (Appel et al., 2013). The aerosol optical properties were estimated by the coated-sphere module (i.e., BHCOAT, Bohren and Huffman, 1983) based on simulated aerosol composition and size distribution (Gan et al., 2015). In the coupled model, the estimated aerosol optical properties are fed to the RRTMG radiation module in WRF, thus updating the simulated atmospheric dynamics which then impact the simulated temperature, photolysis rate, transport, dispersion, deposition and cloud mixing and removal of pollutants. Due to large uncertainties associated with the representation of aerosol impacts on cloud droplet number and optical thickness, the indirect radiative effects of aerosols are not included in the current calculation.

The gridded emission inventory, initial and boundary conditions are consistent with our previous studies (Zhao et al., 2013a, b; Wang et al., 2014), while the simulated domain is extended slightly to cover the entire China, as shown in Figure 1. A better model performance in the simulation of dynamic fields including total solar radiation, PBL height data as well as PM_{2.5} concentrations were suggested after the inclusion of ADE (Wang et al., 2014). In this study, the model performance in the simulation of O₃ will be evaluated through the comparison with observations from 74 cities across China from the China National Urban Air Quality Real-time Publishing Platform (<http://113.108.142.147:20035/emcpublish/>). The simulation period is selected as January 1st to 31st and July 1st to 31st in 2013 to represent winter and summer conditions, respectively. Five regions are selected for analysis, including Jing-Jin-Ji area (denoted JJJ), Yangzi-River-Delta (denoted YRD), Perl-River-Delta (denoted PRD), Sichuan Basin (denoted SCH) and Hubei-Hunan area (denoted HUZ), as shown in Figure 1.

2.2 Simulation Design

Table 1 summarizes the scenario design in this study. In the baseline simulation (denoted SimBL), no aerosol feedbacks either on photolysis rates or radiations was taken into account. In simulation SimNF, only aerosol feedbacks on photolysis rates were considered by embedding an inline photolysis calculation in the model which accounted for modulation of photolysis due to ADE. Finally, in simulation SimSF aerosol feedbacks were considered on both photolysis rates and radiation calculations. Differences between the simulations of SimNF and SimBL are considered as ADE impacts on O₃ through photolysis (denoted Δ Photolysis). Similarly, differences between the simulations of SimSF and SimNF are considered as the ADE impacts on O₃ through dynamics (denoted Δ Dynamics), and differences between the simulations of SimSF and SimBL represents as the combined ADE impacts on O₃ due to both photolysis and dynamics (denoted Δ Total).

10 2.3 Process Analysis

In this study the PA methodology is used in the WRF-CMAQ model to analyze processes impacting simulated O₃ level. The Integrated Process Rates (IPRs) track hourly contributions to O₃ from seven major modeled atmospheric processes that act as sinks or sources of O₃. These processes are gas phase chemistry (denoted CHEM), cloud processes (i.e., the net effect of aqueous-phase chemistry, below- and in-cloud scavenging, and wet deposition, denoted CLDS), dry deposition (denoted DDEP), horizontal advection (denoted HADV), horizontal diffusion (denoted HDIF), vertical advection (denoted ZADV), and turbulent mixing (denoted VDIF). The difference in IPRs among SimBL, SimNF and SimSF represents the response of individual process to ADE. To enable the consistent examination of changes in the process due the ADE across all concentration ranges, we examine changes in the IPRs normalized by the O₃ concentrations. The differences in these process rates (expressed in units of hr⁻¹) between the SimBL, SimSF, SimNF then provide estimates of the changes in process rates resulting from ADE and are shown in the 2nd-4th columns of Figure 4, and (b)-(d) of Figure 5 and 6.

Integrated Reaction Rates (IRRs) are used to investigate the relative importance of various gas-phase reactions in O₃ formation. Following the grouping approach of previous studies (Zhang et al., 2009; Liu et al., 2010; Xing et al., 2011), the chemical production of total odd oxygen (O_x) and the chain length of hydroxyl radical (OH) are calculated. Additionally, the ratio of the chemical production rate of H₂O₂ to that of HNO₃ ($P_{H_2O_2}/P_{HNO_3}$) is an estimated indicator of NO_x- or VOC- limited conditions for O₃ chemistry.

3. Results

3.1 O₃ response to ADE

The simulated surface DMIO₃ in SimBL, SimNF and SimSF are compared in Figure 2a-c. In January, higher DMIO₃ concentrations are seen in PRD where solar radiation is stronger than in the north. The model generally captured the spatial

pattern with highest DMIO₃ in PRD over the simulated domain. Simulated DMIO₃ in YRD, SCH and HUZ are higher than observations. Such overestimation might be associated with the relative coarse spatial resolution in the model. NO titration effects in urban areas were not well represented in the model. In July, high DMIO₃ areas are located towards the north, especially in the JJJ and YRD regions which have relatively larger NO_x and VOC emission density and favorable meteorological condition (e.g., less rain and moderate solar radiation).

In January, O₃ production in north China is occurring in a VOC-limited regime (e.g., Liu et al., 2010), thus increases in NO_x at the surface stemming from the stabilized atmosphere by ADE (Jacobson et al., 2007; Mathur et al., 2010; Ding et al., 2013; Xing et al., 2015) inhibit O₃ formation due to enhanced titration by NO. As seen in Figure 2d, the ΔDynamics reduced DMIO₃ in eastern China by up to 24 μg m⁻³, but slightly increased DMIO₃ in parts of southern China by up to 7 μg m⁻³. The decrease in incoming solar radiation due to ADE significantly reduces the photolysis rates in east China. As seen in Figure 2e, the ΔPhotolysis reduced DMIO₃ domain-wide by up to 16 μg m⁻³. The combined effect of both ΔDynamics and ΔPhotolysis, results in an overall reduction in DMIO₃ as evident across the JJJ and SCH regions with monthly-average reductions up to 39 μg m⁻³.

In July, the O₃ chemistry changes from a VOC-limited to a NO_x-limited regime across most of China. Therefore, increase in NO_x concentration due to the stabilization of atmosphere associated with the ADE, facilitates O₃ formation. The ΔDynamics increased DMIO₃ across most areas of China, particularly in JJJ, YRD and SCH by up to 5 μg m⁻³, with the exception of the PRD region where DMIO₃ decreased. The ΔPhotolysis results in contrasting impacts in July compared to January, as it increased DMIO₃ in most polluted areas including JJJ, YRD, PRD, HUZ, although the solar radiances were reduced due to ΔPhotolysis. This behavior is likely due to enhanced aerosol scattering associated with higher summer-time SO₄²⁻ levels during summer (He and Carmichael, 1999; Jacobson, 1998). Similar results were found in Tie et al (2005) who reported that surface-layer photolysis rates in eastern China were reduced less significantly in summer than in winter. The resultant enhancements in photolysis rates can then cause the noted higher concentrations. More importantly, the diurnal analysis (discussed in the next section) suggested that the reduced photolysis during the early morning in SimNF, enhances the ambient precursor concentrations (due to less reaction in early morning) at noon when O₃ reaches the daily maximum. This increase in precursor concentrations then leads to enhanced O₃ formation later in the day which compensates for or even overwhelms the disbenefit from the reduced solar radiances. In summer, ΔDynamics results in a much stronger influence on DMIO₃ than ΔPhotolysis, and the combined impact of ADE increased O₃ in most of regions in China by up to 4 μg m⁻³.

The impact of the ADE on O₃ is further explored by examining the relationship between the observed and simulated O₃ concentrations (DMIO₃, daily values of the cities located in China) as a function of the observed PM_{2.5} concentrations (observed daily averaged values in those cities), as displayed in Figure 3. The predicted ozone concentrations under both low- and high- PM_{2.5} levels are compared in Table 2. In regards to model performance for DMIO₃ simulations, the model generally

exhibits a slight high bias in January but a low bias in July across the 5 regions. The inclusion of ADE moderately reduced O₃ concentrations in January and slightly increased O₃ in July, resulting in reduction in bias and improved performance for DM1O₃ simulation in both January and July for most of regions. Comparing the O₃ responses to ADE (see Δ-ADE in Table 2) under low- and high- PM_{2.5} levels, reveals that O₃ responses to ADE are larger under high PM_{2.5} levels, indicating the positive correlations between O₃ responses and PM_{2.5} levels.

Interestingly, from low to moderate PM_{2.5} levels (i.e., PM_{2.5} < 120 μg m⁻³), higher O₃ concentration occur with higher PM_{2.5} concentrations, which is evident in both observations and simulations, suggestive of common precursors (e.g., NO_x), source sectors, and/or transport pathways contributing to both O₃ and PM_{2.5} in these regions. However, a negative correlation between O₃ and PM_{2.5} is evident in winter when the PM_{2.5} can reach high levels larger than 120 μg m⁻³, indicating the strong ADE impacts on O₃ through both feedbacks to dynamics and photolysis which significantly reduced O₃.

3.2 IPRs response to ADE

To further explore the ADE impacts on simulated O₃, the integrated process contributions are further analyzed in three ways: (a) 24-hour diurnal variations of process contributions to simulated surface O₃ (Figure 4), (b) vertical profiles from ground up to 1357 m AGL (above ground level, in model layer 1-10) at noon (Figure 5), and (c) correlations with near-ground PM_{2.5} (average concentrations between the ground and 355m AGL, model layer 1-5) (Figure 6). In the following, we limit our discussion to analysis of model results for the JJJ region which exhibited the strongest ADE among the regions; similar results were found for the other 4 regions and can be found in the Supporting Information section.

Diurnal variation of process contributions from chemistry (CHEM), dry deposition (DDEP) and vertical turbulent mixing (VDIF) which together contribute to more than 90% of the O₃ rate of change for the JJJ region, are illustrated in Figure 4. The diurnal variation of IPRs for other processes and their response to ADE are displayed in Figure S1 for JJJ and Figure S2-S5 for other 4 regions.

For surface-level O₃, VDIF is the major source and DDEP is the major sink (Figure S1). The stabilization of atmosphere due to ΔDynamics leads to lower dry deposition rates (due to lower dry deposition velocity from the enhanced aerodynamic resistance) and thus increases surface O₃. The largest impact of ΔDynamics on DDEP occurs during early morning and late afternoon which is consistent with the response of the PBL height to ADE noted in our previous analysis (Xing et al., 2015).

Expectedly, CHEM is the second largest sink for surface O₃ during January, but a source for surface O₃ during the daytime in July. The ΔDynamics increased the surface O₃ around noon in both January and July for almost all regions (no impacts in PRD and YRD in January, see Figure S2-S3), since increased stability due to ΔDynamics concentrated more precursors locally, leading to enhanced O₃ formation during the photochemically most active period of the day. The ΔDynamics reduced the surface O₃ around late afternoon in January at all regions. This is because the increased atmospheric stability during late

afternoon and evening hours increased NO_x concentration which titrated more O_3 . The $\Delta\text{Photolysis}$ reduced surface O_3 in all regions in January. These reductions were more pronounced during the early morning hours when the photolysis rate are most sensitive to the radiation intensity. The $\Delta\text{Photolysis}$ resulted in comparatively larger reductions in surface O_3 during the early morning and late afternoon hours in July, but slightly increased surface O_3 at noon for most of the regions. This increase in O_3 can be hypothesized to result from the following sequence of events. Slower photochemical reaction in the morning in the $\Delta\text{Photolysis}$ case lead to higher levels of precursors, whose accumulation then enhances O_3 formation at noon. This hypothesis is further confirmed by the changes in the diurnal variation of NO_2 which suggest that higher NO to NO_2 conversion during early morning results in enhanced daytime NO_2 levels (see Figure S6), consequently leading to higher noon-time O_3 .

For aloft O_3 (from 100 to 1600 meters above ground) as seen in Figure 5, CHEM is the major source for O_3 at noon both in January and in July. The $\Delta\text{Dynamics}$ increased near-surface O_3 (below 500m, model layer 1-6), but reduced upper-level O_3 (above 500m, model layer 7-10), because increased stability of the atmosphere concentrated precursors emissions within a shallower layer resulting in higher O_3 production. The $\Delta\text{Photolysis}$ case considerably reduced near-surface O_3 at noon in January. In July, $\Delta\text{Photolysis}$ increased upper-level O_3 at noon. Higher levels of precursors at noon might be the reason for such enhancement (see Figure S6).

The daytime near-ground-averaged (between the ground and 350m AGL, layers 1-5) IPR responses to ADE are shown in Figure 6 for JJJ and in Figure S7 for other regions. The IPR and its responses are presented as a function of near-ground-averaged $\text{PM}_{2.5}$ concentrations. As shown in Figure 6, as $\text{PM}_{2.5}$ concentrations increase, the positive contribution of CHEM in July become larger while the negative contribution of CHEM in January become smaller. The overall ADE enhanced CHEM and thus increased O_3 concentration in July, and such enhancement are generally larger for higher $\text{PM}_{2.5}$ loading. In contrast, in January overall ADE resulted in higher rates of O_3 destruction due to chemistry (negative contribution of CHEM), and the magnitude of this sink increased as $\text{PM}_{2.5}$ concentrations increase. The reduction of O_3 stemming from the enhancements in the chemical sinks is the dominant impact of ADE in January. The enhanced positive contribution of CHEM due to $\Delta\text{Dynamics}$ was partially compensated by the reduction from $\Delta\text{Photolysis}$ (see Figure S7), resulting in a slight increase in the positive CHEM contribution to O_3 in July.

DDEP is the major sink of daytime O_3 during both January and July. The increased stability due to ADE reduced deposition velocity and thus increases O_3 . These effects become larger with increasing $\text{PM}_{2.5}$ concentrations. Thus, weaker removal of O_3 from DDEP associated with ADE, contributed to higher O_3 in most regions during both January and July. Enhanced O_3 source of CHEM and reduced O_3 sink of DDEP is the dominant impact of ADE in July.

3.3 IRR response to ADE

The simulated mid-day average (11:00-13:00 local time) surface O_x (defined as the sum of O , O_3 , NO_2 , NO_3 , N_2O_5 , HNO_3 , PNA , NTR , PAN and PANX) and OH and their responses to ADE are shown in Figure 7. Both O_x and OH are significantly

reduced in the Δ Photolysis case in January throughout the modeling domain. Both O_x and OH also show reductions in the middle portions of east China in the Δ Dynamics case in January. Together, the combined ADE impacts result in reduced O_x and OH in January, with widespread reductions primarily due to ADE on photolysis. In July, Δ Photolysis increased mid-day OH across most of China (Figure 7) which is consistent with the increase of O_3 at noon stemming from a higher level of precursors accumulation due to Δ Photolysis. The overall ADE impact on OH is controlled by Δ Photolysis, and result in increased mid-day OH across most of China. For O_x , however, the impact of Δ Dynamics overwhelms the impact from Δ Photolysis, resulting in increase in O_x concentrations in east China including YRD, SCH and HUZ.

To further examine the response of O_x to ADE, in Figure 8 we examine vertical profiles of the integrated reaction rates at noon for the JJJ region. The stabilization of the atmosphere due to Δ Dynamics concentrates precursors within a lower PBL, resulting in an increased total O_x production rate (P_{totalO_x}) mostly in near-ground model layers (below 500m, model layer 1-6); in magnitude aloft (above 500m, model layer 7-10), this change in P_{totalO_x} is smaller in January, and become decreasing in July. The reduction of P_{totalO_x} due to Δ Photolysis is greatest at the surface in January, and declines with altitude, and even becomes reversed at high layers (about 1300m, model layer 10) (Figure 8a). The overall ADE impact in January is mainly dominated by Δ Photolysis which largely overwhelms the impact of Δ Dynamics (Figure 8a). However, in July, Δ Photolysis enhanced P_{totalO_x} across all layers. The P_{totalO_x} shows small decreases at high altitudes but significant increase in near-ground model layers (below 500m, model layer 1-6) due to the combined ADE in July.

The changes in vertical profiles of production rates of new OH (P_{NewOH}) and reacted OH ($P_{ReactedOH}$) are similar to those of P_{totalO_x} , with the noted decreases in January dominated by Δ Photolysis. In contrast, the increases in July result from contribution from both Δ Photolysis and Δ Dynamics.

Analysis of the chain length is important to understand the characteristics of chain reaction mechanisms. The OH chain length (denoted OH_CL) is determined by the ratio of $P_{ReactedOH}$ to P_{NewOH} . Δ Dynamics concentrated more NO_x at surface, thus leading to an increased OH_CL (i.e., more reacted OH than new OH) in the near-ground layers, but a decreased OH_CL in the upper layers. In January, the Δ Photolysis reduced P_{NewOH} more than $P_{ReactedOH}$ (probably because of more abundance of NO_x resulting from photolysis attenuation and consequently reduced photochemistry), thereby leading to an increased OH_CL. In July, Δ Photolysis enhanced both P_{NewOH} and $P_{ReactedOH}$, particularly in the upper layers. The OH_CL is increased by Δ Photolysis because higher NO_x levels (see Figure S6) cause more reacted OH to be reacted. Thus the surface OH_CL at noon is increased in both January and July from combined ADE of Δ Photolysis and Δ Dynamics, indicating a stronger propagation efficiency of the chain.

The production rates of H_2O_2 ($P_{H_2O_2}$) and HNO_3 (P_{HNO_3}) and their responses to ADE are also summarized in Figure 8 (average for mid-day hours) for the JJJ region (similar illustrations for the other regions can be found in the supplemental Figures S8-S11. Smaller ratios of $P_{H_2O_2}/P_{HNO_3}$ are noted in January compared to July, indicating a stronger VOC-limited regime in January

for all regions. The Δ Dynamics increases P_{HNO_3} but decreases $P_{\text{H}_2\text{O}_2}$ in both January and July because the enhanced NO_x at the surface in a more stable atmosphere likely shifts O_3 chemistry towards NO_x -rich condition. The Δ Photolysis reduced both $P_{\text{H}_2\text{O}_2}$ and P_{HNO_3} but the ratio of $P_{\text{H}_2\text{O}_2}/P_{\text{HNO}_3}$ is decreased due to larger reduction in $P_{\text{H}_2\text{O}_2}$ than P_{HNO_3} . The combined impacts of Δ Dynamics and Δ Photolysis result in a shift towards more VOC-limited conditions in the near-surface layers during both
5 January and July.

4. Summary

The impacts of ADE on tropospheric ozone were quantified by using the two-way coupled meteorology and atmospheric chemistry WRF-CMAQ model instrumented with the process analysis methodology. Two manifestations of ADE impacts on O_3 , changes in atmospheric dynamics (Δ Dynamics) and changes in photolysis rates (Δ Photolysis), were systematically
10 evaluated through simulations that isolated their impacts on modeled process rates over China for winter and summer conditions (represented by the months of January and July in 2013, respectively). Results suggest that the model performance for surface DMIO_3 simulations improved after the inclusion of ADE which moderately reduced the high-bias in January and low-bias in July. In winter, the inclusion of ADE impacts resulted in an overall reduction in surface DMIO_3 across China by up to $39 \mu\text{g m}^{-3}$. Changes both in photolysis and atmospheric dynamics due to ADE contributed to the reductions in DMIO_3
15 in winter. In contrast during July, the impact of ADE increased surface DMIO_3 across China by up to $4 \mu\text{g m}^{-3}$. The summertime increase in DMIO_3 results primarily from ADE induced effects on atmospheric dynamics. It can thus be postulated that reducing ADE will have potential risk of increasing O_3 in winter, but will benefit the reduction of maximum O_3 in summer.

Results from IPR analysis suggest that the ADE impacts exhibit strong vertical and diurnal variations. The ADE induced
20 decrease in modeled DMIO_3 in January primarily results from Δ Photolysis which reduced the chemical production of O_3 in the near-ground layers. The increase in DMIO_3 in July due to ADE results from a weaker dry deposition sink as well as a stronger chemical source due to higher precursor concentrations in a more stable and shallow PBL. These impacts become stronger under higher $\text{PM}_{2.5}$ concentrations when ADE are larger.

The combined ADE impacts reduce O_x in January due to Δ Photolysis, but slightly increase O_x in July due to Δ Dynamics. OH
25 is reduced by ADE in January. However, mid-day OH concentrations during summertime show enhancements associated with both Δ Photolysis and Δ Dynamics, indicating a stronger mid-day atmospheric oxidizing capacity in July. An increased OH chain length in the near-ground layers is modeled both in January and July, indicating a stronger propagation efficiency of the chain reaction. In both January and July, P_{HNO_3} is increased and $P_{\text{H}_2\text{O}_2}$ is decreased due to Δ Dynamics, and both are reduced due to Δ Photolysis. The ratio of $P_{\text{H}_2\text{O}_2}/P_{\text{HNO}_3}$ is decreased due to the combined impacts of Δ Dynamics and Δ Photolysis,
30 indicating a shift towards more VOC-limited conditions due to ADE in the near-ground layers during both January and July.

Thus aerosol direct effects on both photolysis rates as well as atmospheric dynamics can impact O₃ formation rates and its local and regional distributions. Comparisons of integrated process rates suggest that the decrease in DMIO₃ in January results from a larger net chemical sink due to ΔPhotolysis, while the increase in DMIO₃ in July is mostly associated with the slower removal due to reduced deposition velocity as well as a stronger photochemistry due to ΔDynamics. The IRR analyses confirm that the process contributions from chemistry to DMIO₃ can be influenced by both ΔDynamics and ΔPhotolysis. Reduced ventilation associated with ΔDynamics enhances the precursor levels, which increase chemical production rate of O_x and OH, resulting in greater O₃ chemical formation at noon during both January and July. On the other hand, reduced photolysis rates in ΔPhotolysis results in lower O₃ in January. However, in July lower photolysis rates result in accumulation of precursors during the morning hours which eventually lead to higher O₃ production at noon.

The comparison of integrated reaction rates from the various simulations also suggest that the increased OH_{CL} and the shift towards more VOC-limited conditions are mostly associated with the higher NO₂ levels due to ADE. This further emphasizes the importance of NO_x controls in air pollution mitigation. Traditionally, the co-benefits from NO_x control for ozone and PM reduction are mostly because that NO_x is a common precursor for both O₃ and PM_{2.5}. This study suggests that effective controls on NO_x will not only gain direct benefits for O₃ reduction, but also can indirectly reduce peak O₃ through weakening the ADE from the reduced PM_{2.5}, highlighting co-benefits from NO_x controls for achieving both O₃ and PM_{2.5} reductions.

Reducing aerosols will have substantial impacts on ozone. Quantification of the aerosol influence on ozone is important to understand co-benefits associated with reductions in both particulate matter and ozone. This study focused on the evaluation of ADE impacts which were not well quantified previously. However, the heterogeneous reactions associated with aerosols, as well as the impacts of emission controls of gaseous precursors on both aerosols and ozone also need to be studied in order to fully understand the influence from reducing aerosols on ambient ozone.

Acknowledgements

This work was supported in part by MEP's Special Funds for Research on Public Welfare (201409002), MOST National Key R & D program (2016YFC0203306) and MOST National Key R & D program (2016YFC0207601). This work was completed on the "Explorer 100" cluster system of Tsinghua National Laboratory for Information Science and Technology.

Disclaimer: Although this work has been reviewed and approved for publication by the U.S. Environmental Protection Agency, it does not necessarily reflect the views and policies of the agency.

References

Albrecht, B.A., Aerosols, Cloud Microphysics, and Fractional Cloudiness. *Science*, 245, 1227-1230, 1989.

- Anger, A., Dessens, O., Xi, F., Barker, T., and Wu, R.: China's air pollution reduction efforts may result in an increase in surface ozone levels in highly polluted areas. *Ambio*, 45:254–265, 2016.
- Appel, K. W., Pouliot, G.A., Simon, H., Sarwar, G., Pye, H.O.T., Napelenok, S.L., Akhtar, F., Roselle, S.J.: Evaluation of dust and trace metal estimates from the Community Multiscale Air Quality (CMAQ) model version 5.0, *Geosci. Model Dev.*, 6, 883-899, doi:10.5194/gmd-6-883-2013, 2013.
- Benas, N., Mourtzanou, E., Kouvarakis, G., Bais, A., Mihalopoulos, N., and Vardavas, I.: Surface ozone photolysis rate trends in the Eastern Mediterranean: Modeling the effects of aerosols and total column ozone based on Terra MODIS data. *Atmospheric Environment*, 74, 1-9, 2013.
- Bian, H., Han, S., Tie, X., Sun, M. and Liu, A.: Evidence of impact of aerosols on surface ozone concentration in Tianjin, China. *Atmospheric Environment*, 41(22), 4672-4681, 2007.
- Bohren, C.F.; Huffman, D.R. *Absorption and Scattering of Light by Small Particles*. Wiley-Interscience, New York, 530, 1983.
- Davis, J. M., Bhave, P. V., and Foley, K. M.: Parameterization of N₂O₅ reaction probabilities on the surface of particles containing ammonium, sulfate, and nitrate, *Atmos. Chem. Phys.*, 8, 5295–5311, doi:10.5194/acp-8-5295-2008, 2008.
- Dickerson, R.R., Kondragunta, S., Stenchikov, G., Civerolo, K.L., Doddridge, B.G. and Holben, B.N.: The impact of aerosols on solar ultraviolet radiation and photochemical smog. *Science*, 278(5339), 827-830, 1997.
- Ding, A.J., Huang, X., Nie, W., Sun, J.N., Kerminen, V.M., Petäjä, T., Su, H., Cheng, Y.F., Yang, X.Q., Wang, M.H., Chi, X.G., Wang, J.P., Virkkula, A., Guo, W.D., Yuan, J., Wang, S.Y., Zhang, R.J., Wu, Y.F., Song, Y., Zhu, T., Zilitinkevich, S. and Kulmala, M.: Black carbon enhances haze pollution in megacities in China, *Geophysical Research Letters*, 43, 2016.
- Gan, C.M., Hogrefe, C., Mathur, R., Pleim, J., Xing, J., Wong, D., Gilliam, R., Pouliot, G., Wei, C.: Assessment of the aerosol optics component of the coupled WRF-CMAQ model using CARES field campaign data and a single column model. *Atmos. Environ.*, 115, 670-682, 2015.
- Haagen-Smit, A. J., and Fox, M. M.: Photochemical ozone formation with hydrocarbons and automobile exhaust, *Air Repair* 4, no. 3, 105-136, 1954.
- Hansen, J., Sato, M., Ruedy, R., *Radiative forcing and climate response. J Geophys Res-Atmos*, 102, 6831-6864, 1997.
- He, S. and Carmichael, G.R.: Sensitivity of photolysis rates and ozone production in the troposphere to aerosol properties. *Journal of Geophysical Research: Atmospheres*, 104(D21), 26307-26324, 1999.
- Hogrefe, C., Pouliot, G., Wong, D., Torian, A., Roselle, S., Pleim, J. and Mathur, R.: Annual application and evaluation of the online coupled WRF-CMAQ system over North America under AQMEII phase 2. *Atmospheric Environment*, 115, 683-694, 2015.
- Jacobson, M.Z.: Studying the effects of aerosols on vertical photolysis rate coefficient and temperature profiles over an urban airshed. *Journal of Geophysical Research*, 103(D9), pp.10593-10604, 1998.

- Jacobson, M. Z.: Control of fossil-fuel particulate black carbon plus organic matter, possibly the most effective method of slowing global warming, *J. Geophys. Res.*, 107 (D19), 4410, 2002, doi:10.1029/2001JD001376.
- Jacobson, M. Z., Kaufman, Y. J. and Rudich, Y.: Examining feedbacks of aerosols to urban climate with a model that treats 3-D clouds with aerosol inclusions, *J. Geophys. Res.*, 112, D24205, 2007.
- 5 Jacobson, M.Z.: Short-term effects of controlling fossil-fuel soot, biofuel soot and gases, and methane on climate, Arctic ice, and air pollution health, *J. Geophys. Res.*, 115, D14209, 2010, doi:10.1029/2009JD013795.
- Li, J., Wang, Z., Wang, X., Yamaji, K., Takigawa, M., Kanaya, Y., Pochanart, P., Liu, Y., Irie, H., Hu, B. and Tanimoto, H., Impacts of aerosols on summertime tropospheric photolysis frequencies and photochemistry over Central Eastern China. *Atmospheric Environment*, 45, 1817-1829, 2011.
- 10 Liao, H., Seinfeld, J.H., Global impacts of gas-phase chemistry–aerosol interactions on direct radiative forcing by anthropogenic aerosols and ozone, *J. Geophys. Res.*, 110, D18208, 2005.
- Liou, K., Ou, S., The role of cloud microphysical processes in climate - an assessment from a one-dimensional perspective. . *J Geophys Res-Atmos*, 94, 8599-8607, 1989.
- Liu, X.H., Zhang, Y., Xing, J., Zhang, Q., Wang, K., Streets, D.G., Jang, C., Wang, W.X. and Hao, J.M.: Understanding of regional air pollution over China using CMAQ, part II. Process analysis and sensitivity of ozone and particulate matter to precursor emissions. *Atmospheric Environment*, 44(30), pp.3719-3727, 2010.
- 15 Lou S. J., Liao H., Zhu B. Impacts of aerosols on surface-layer ozone concentrations in China through heterogeneous reactions and changes in photolysis rates. *Atmospheric Environment*, 48: 123-138, 2014.
- Mathur, R., Pleim, J., Wong, D., Otte, T. L., Gilliam, R. C., Roselle, S.J., Young, J. O., Binkowski, F. S., and Xiu, A.: The WRF-CMAQ Integrated On-Line Modeling System: Development, Testing, and Initial Applications. Chapter 2, Douw G. Steyn and S. T. Rao (ed.), *Air Pollution Modeling and its Applications XX* (pp. 155-159). Springer Netherlands, Netherlands, 2010.
- 20 Mitchell, J.F.B., Davis, R.A., Ingram, W.J., Senior, C.A., On Surface Temperature, Greenhouse Gases, and Aerosols: Models and Observations. *Journal of Climate* 1995; 8: 2364-2386.
- Pleim, J., Young, J., Wong, D., Gilliam, R., Otte, T., and Mathur, R.: Two-Way Coupled Meteorology and Air Quality Modeling, *Air Pollution Modeling and Its Application XIX*, NATO Science for Peace and Security Series C: Environmental Security, 2, 235-242, 2008.
- Pozzoli, L., Bey, I., Rast, S., Schultz, M.G., Stier, P., Feichter, J., Trace gas and aerosol interactions in the fully coupled model of aerosol-chemistry-climate ECHAM5-HAMMOZ: 1. Model description and insights from the spring 2001 TRACE-P
- 30 experiment, *J. Geophys. Res.*, 113, D07308, 2008.

- Sarwar, G., Luecken, D., Yarwood, G., Whitten, G.Z., Carter, W.P.: Impact of an updated carbon bond mechanism on predictions from the CMAQ modeling system: Preliminary assessment. *Journal of applied meteorology and climatology*, 47, 3-14, 2008.
- Sarwar, G., Simon, H., Bhawe, P., and Yarwood, G.: Examining the impact of heterogeneous nitryl chloride production on air quality across the United States, *Atmospheric Chemistry & Physics*, 12, 1-19, 2012.
- Sarwar, G., Simon, H., Xing, J., Mathur, R.: Importance of tropospheric ClNO₂ chemistry across the Northern Hemisphere, *Geophysical Research Letters*, 41, 4050-4058, 2014.
- Tang, Y., Carmichael, G.R., Kurata, G., Uno, I., Weber, R.J., Song, C.H., Guttikunda, S.K., Woo, J.H., Streets, D.G., Wei, C. and Clarke, A.D., Impacts of dust on regional tropospheric chemistry during the ACE-Asia experiment: A model study with observations. *Journal of Geophysical Research-Atmospheres*, 109, 2004.
- Tie, X., Madronich, S., Walters, S., Edwards, D.P., Ginoux, P., Mahowald, N., Zhang, R., Lou, C. and Brasseur, G., Assessment of the global impact of aerosols on tropospheric oxidants. *Journal of Geophysical Research-Atmospheres*, 110(D3), 2005.
- Twomey, S., Influence of pollution on shortwave albedo of clouds. *Journal of the Atmospheric Sciences*, 34, 1149-1154, 1977.
- Wang, J., Wang, S., Jiang, J., Ding, A., Zheng, M., Zhao, B., Wong, D.C., Zhou, W., Zheng, G., Wang, L. and Pleim, J.E.: Impact of aerosol–meteorology interactions on fine particle pollution during China’s severe haze episode in January 2013. *Environ. Res. Lett.*, 9, 094002, 2014.
- Wang, J., Allen, D. J., Pickering, K. E., Li, Z. and He, H.: Impact of aerosol direct effect on East Asian air quality during the EAST-AIRE campaign, *J. Geophys. Res. Atmos.*, 121, 2016, doi:10.1002/2016JD025108.
- Wang, J., Zhao, B., Wang, S., Yang, F., Xing, J., Morawska, L., Ding, A., Kulmala, M., Kerminen, V.M., Kujansuu, J. and Wang, Z.: Particulate matter pollution over China and the effects of control policies. *Science of the Total Environment*, 584-585: 426-447, 2017.
- Wong, D. C., Pleim, J., Mathur, R., Binkowski, F., Otte, T., Gilliam, R., Pouliot, G., Xiu, A., Young, J. O., and Kang, D.: WRF-CMAQ two-way coupled system with aerosol feedback: software development and preliminary results, *Geosci. Model Dev.*, 5, 299-312, doi:10.5194/gmd-5-299-2012, 2012.
- Xing, J., Zhang, Y., Wang, S., Liu, X., Cheng, S., Zhang, Q., Chen, Y., Streets, D.G., Jang, C., Hao, J. and Wang, W.: Modeling study on the air quality impacts from emission reductions and atypical meteorological conditions during the 2008 Beijing Olympics. *Atmospheric Environment*, 45(10), 1786-1798. 2011.
- Xing, J., Mathur, R., Pleim, J., Hogrefe, C., Gan, C.M., Wong, D.C., Wei, C. and Wang, J.: Air pollution and climate response to aerosol direct radiative effects: a modeling study of decadal trends across the northern hemisphere. *J. Geophys. Res.*, 120, 12,221–12,236, 2015a.

- Xing, J., Mathur, R., Pleim, J., Hogrefe, C., Gan, C.-M., Wong, D. C., and Wei, C.: Can a coupled meteorology-chemistry model reproduce the historical trend in aerosol direct radiative effects over the Northern Hemisphere?, *Atmos. Chem. Phys.*, 15, 9997-10018, doi:10.5194/acp-15-9997-2015, 2015b.
- Xu, J., Zhang, Y.H., Zheng, S.Q., He, Y.J., *Aerosol effects on ozone concentrations in Beijing: a model sensitivity study*, *J. Environ. Sci.*, 24 (4), 645–656, 2012.
- 5 Yu, S., Mathur, R., Pleim, J., Wong, D., Gilliam, R., Alapaty, K., Zhao, C., and Liu, X.: Aerosol indirect effect on the grid-scale clouds in the two-way coupled WRF-CMAQ: model description, development, evaluation and regional analysis, *Atmos. Chem. Phys. Discuss.*, 13, 25649-25739, doi:10.5194/acpd-13-25649-2013, 2013.
- Zhang, Y., Wen, X.Y., Wang, K., Vijayaraghavan, K. and Jacobson, M.Z.: Probing into regional O₃ and particulate matter
10 pollution in the United States: 2. An examination of formation mechanisms through a process analysis technique and sensitivity study. *Journal of Geophysical Research: Atmospheres*, 114(D22), 2009.
- Zhao, B., Wang, S., Dong, X., Wang, J., Duan, L., Fu, X., Hao, J. and Fu, J.: Environmental effects of the recent emission changes in China: implications for particulate matter pollution and soil acidification. *Environmental Research Letters*, 8(2), 024031, 2013a.
- 15 Zhao, B., Wang, S., Wang, J., Fu, J.S., Liu, T., Xu, J., Fu, X. and Hao, J.: Impact of national NO_x and SO₂ control policies on particulate matter pollution in China. *Atmospheric Environment*, 77, 453-463, 2013b.

Table 1: Description of sensitivity simulations in this study

Short name	Simulation description	Aerosol impacts on photolysis calculations	Aerosol impacts on radiation calculations
SimBL	Baseline simulation	No	No
SimNF	No aerosol feedback simulation	Yes	No
SimSF	Aerosol feedback simulation	Yes	Yes

Table 2: Comparison of model performance in ozone prediction across three simulations (monthly average of daily 1h maxima)

Region	OBS ($\mu\text{g m}^{-3}$)	Low PM _{2.5} (<60 $\mu\text{g m}^{-3}$) Normalized Mean Bias			Δ -ADE* ($\mu\text{g m}^{-3}$)	OBS ($\mu\text{g m}^{-3}$)	High PM _{2.5} (>60 $\mu\text{g m}^{-3}$) Normalized Mean Bias			Δ -ADE ($\mu\text{g m}^{-3}$)	
		SimSF	SimNF	SimBL			SimSF	SimNF	SimBL		
January	JJJ	62.52	3%	4%	5%	-1.05	37.02	22%	36%	53%	-11.36
	YRD	63.89	38%	41%	43%	-2.76	66.74	54%	59%	67%	-8.85
	PRD	97.25	25%	26%	29%	-4.52	122.61	6%	5%	9%	-4.63
	HUZ	47.67	172%	173%	193%	-10.17	67.29	107%	125%	142%	-23.9
	SCH	88.63	-43%	-40%	-38%	-3.85	111.19	-5%	2%	8%	-13.78
	China	76.61	30%	31%	34%	-2.96	62.68	42%	48%	56%	-8.61
July	JJJ	159.27	-29%	-28%	-28%	-0.51	178.54	-25%	-25%	-25%	1.02
	YRD	171.04	-31%	-31%	-32%	0.84	233.13	-24%	-25%	-23%	-0.51
	PRD	129.02	-20%	-19%	-20%	-0.09	312.21	-44%	-45%	-46%	4.92
	HUZ	187.44	-36%	-37%	-37%	1.39	208.99	-27%	-28%	-29%	4.19
	SCH	163.81	-38%	-38%	-39%	0.77	191.19	-30%	-31%	-31%	1.18
	China	145.24	-28%	-28%	-28%	0.3	181.65	-25%	-25%	-25%	0.9

* Δ -ADE represents the O₃ response to ADE which is calculated from the difference between SimSF and SimBL.

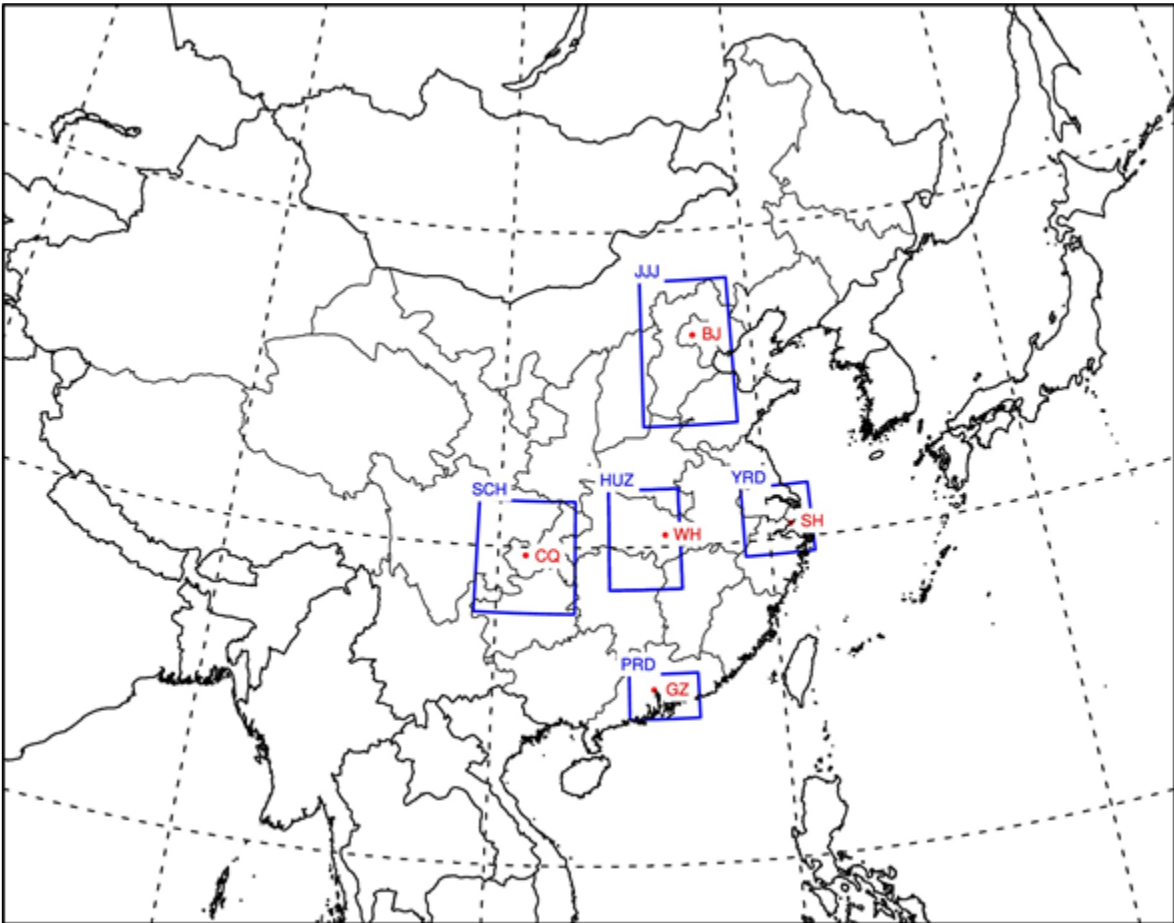


Figure 1: Simulation domain and locations of 5 selected regions in China. Note: JJJ=Jing-Jin-Ji area, YRD=Yangzi-River-Delta area, PRD=Perl-River-Delta area, SCH=Sichuan Basin area, HUZ=Hubei-Hunan area.

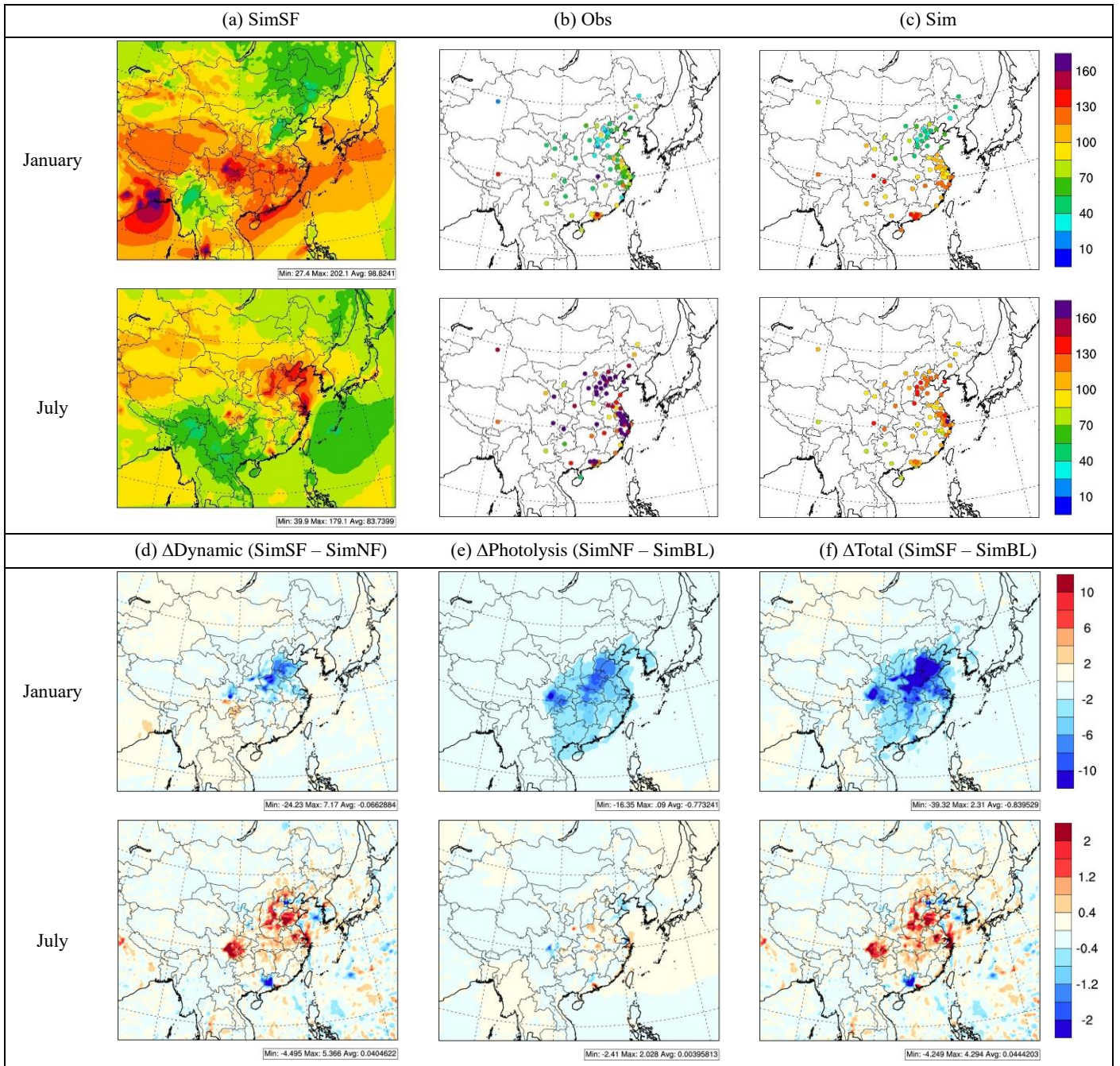


Figure 2: Observed and simulated O_3 and its response to ADE (monthly average of daily 1h maxima, $\mu g m^{-3}$)

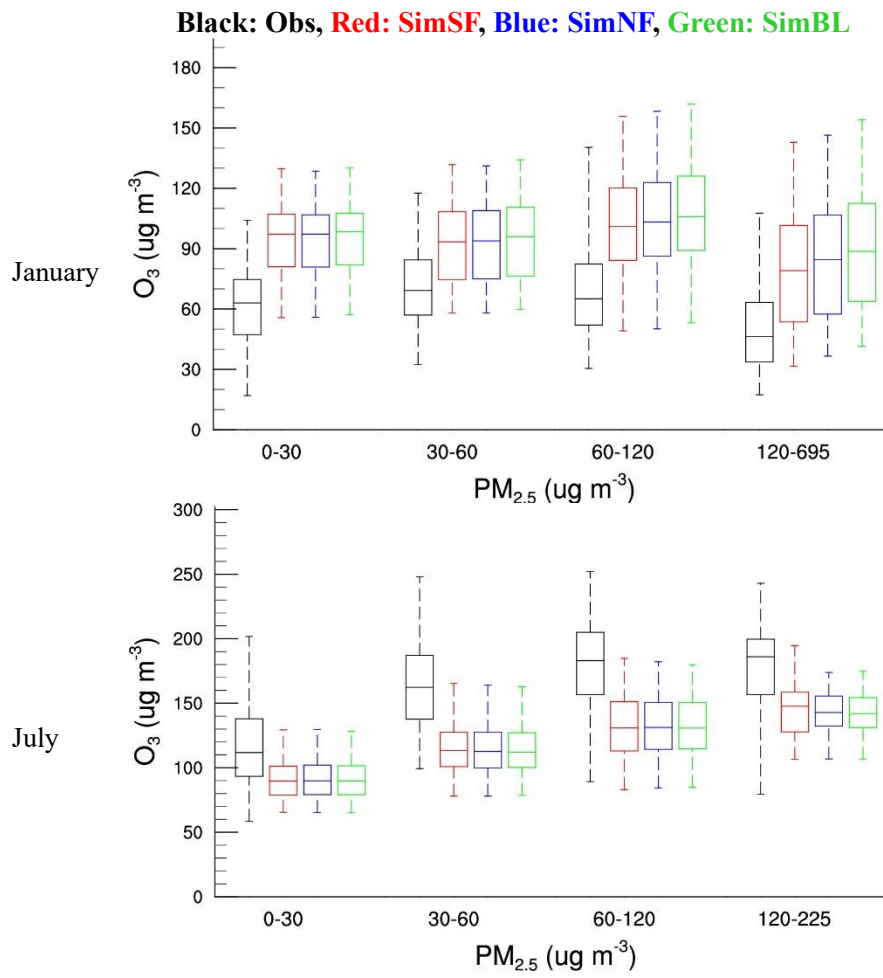


Figure 3: Observed and simulated surface O₃ concentration against PM_{2.5} concentration (O₃ is daily 1h maxima of monitor sites over China, unit: $\mu\text{g m}^{-3}$; PM_{2.5} is the daily average of those site, unit: $\mu\text{g m}^{-3}$)

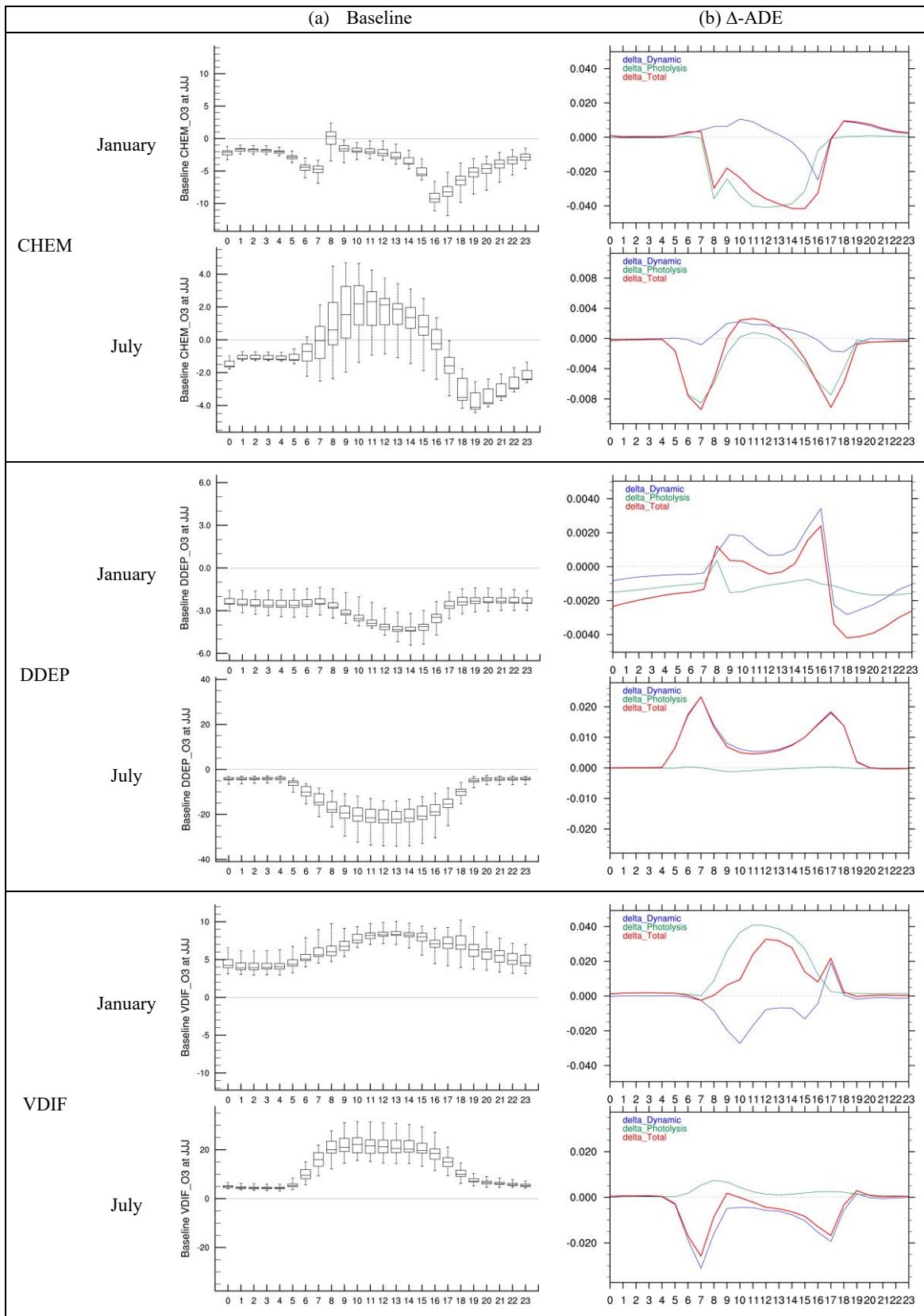


Figure 4: Diurnal variation of selected integrated process contributions to surface O_3 concentration in JJJ (The calculation is based on the average of grid cells in JJJ; a. Baseline is the simulated O_3 in SimBL, unit: ppb hr^{-1} ; b. Δ -ADE is the difference in normalized IPRs between simulations, unit: hr^{-1} : delta_Dynamic is the difference between SimSF and SimNF, delta_Photolysis is the difference between SimNF and SimBL, delta_Total is the difference between SimSF and SimBL)

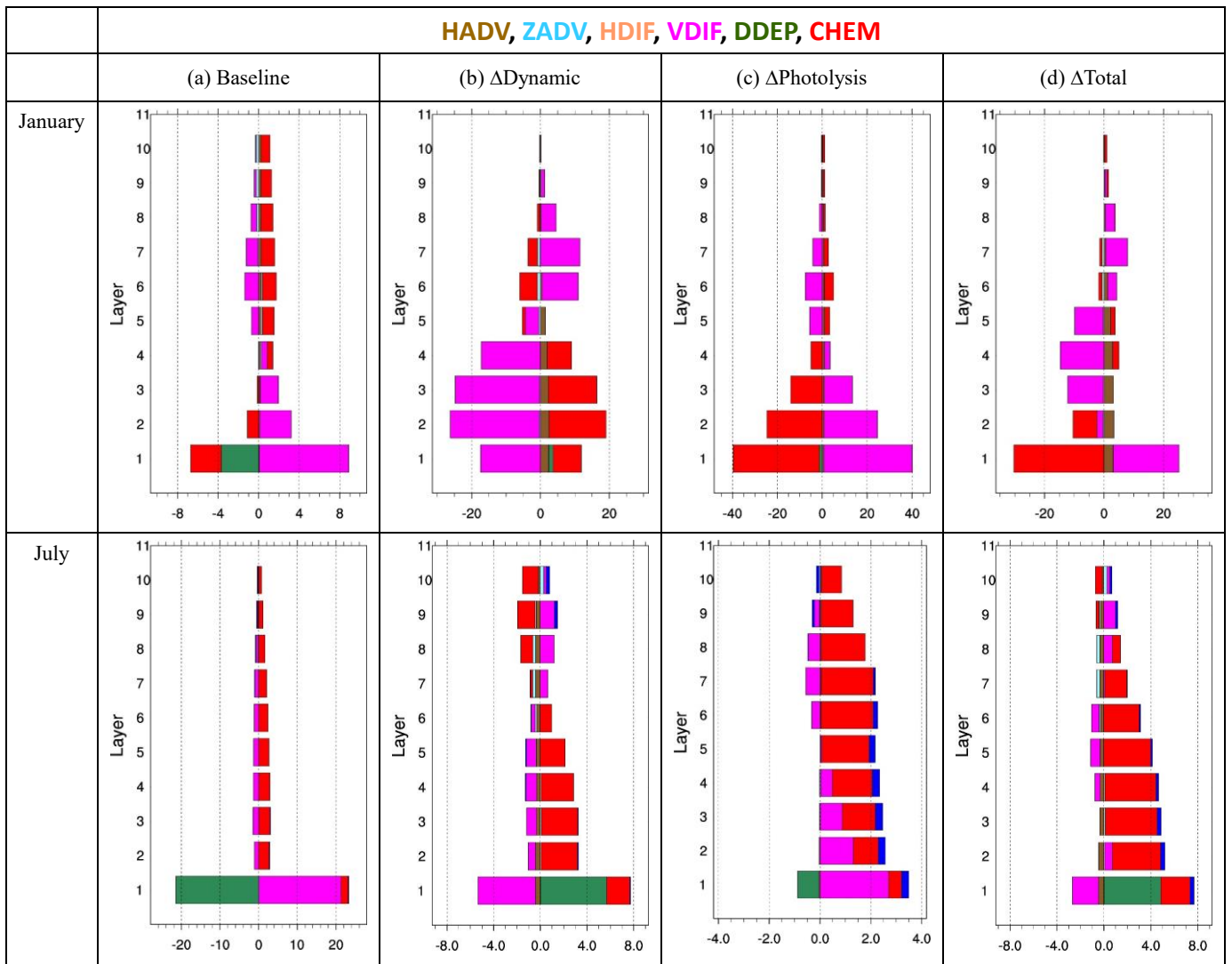


Figure 5: Vertical profile of integrated process contributions to surface O_3 concentration at noon in JJJ (full-layer heights above ground are 40, 96, 160, 241, 355, 503, 688, 884, 1100, 1357m; a. Baseline is the simulated O_3 in SimBL, unit: $ppb\ hr^{-1}$; b. Δ Dynamic is the difference in normalized IPRs between SimSF and SimNF, unit: hr^{-1} ; d. Δ Photolysis is the difference in normalized IPRs between SimNF and SimBL, unit: hr^{-1} ; c. Δ Total is the difference in normalized IPRs between SimSF and SimBL, unit: hr^{-1})

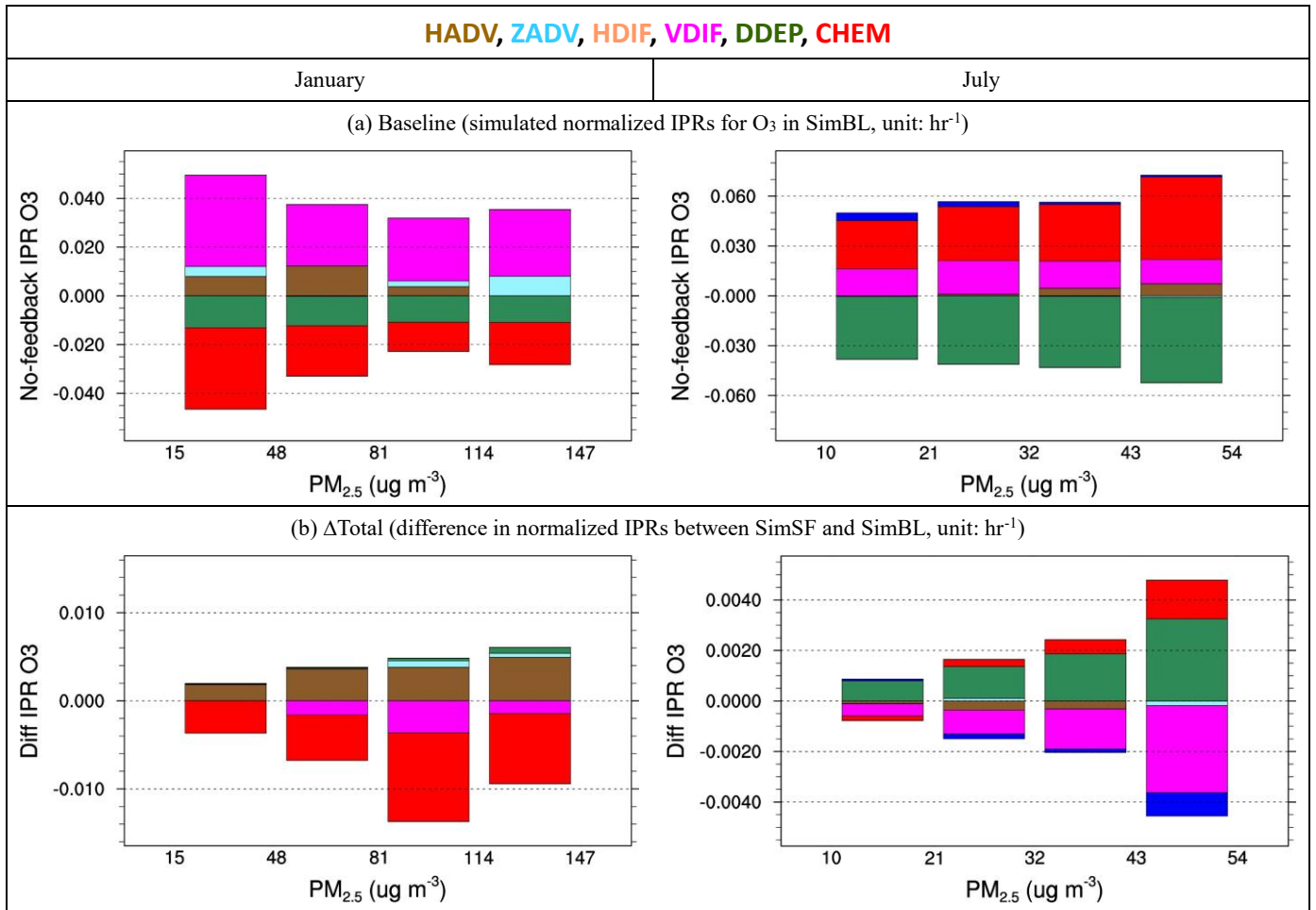


Figure 6: Integrated process contributions to daytime near-ground-level O₃ under different PM_{2.5} level in JJJ (between the ground and 350m AGL, model layer 1-5)

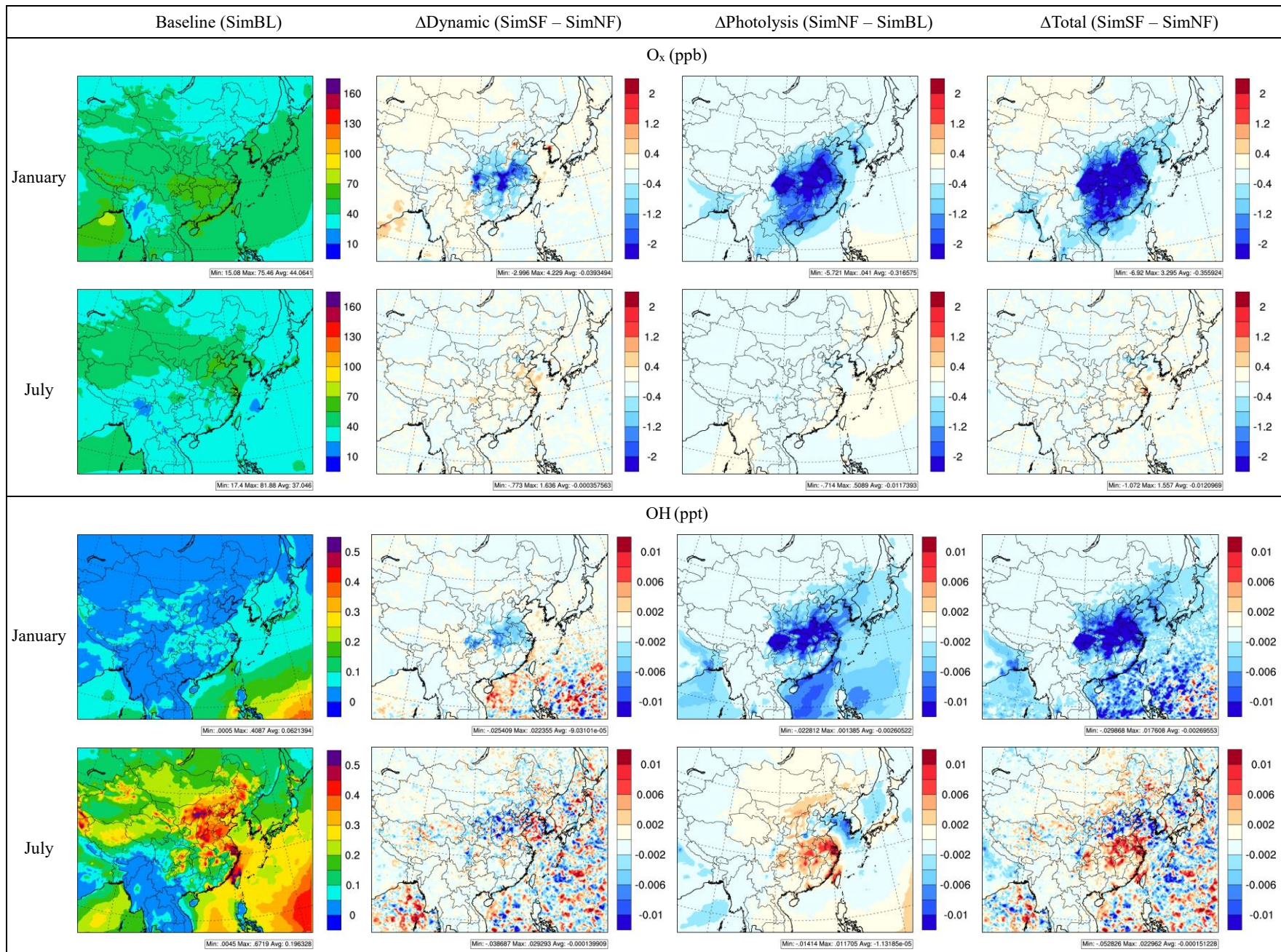
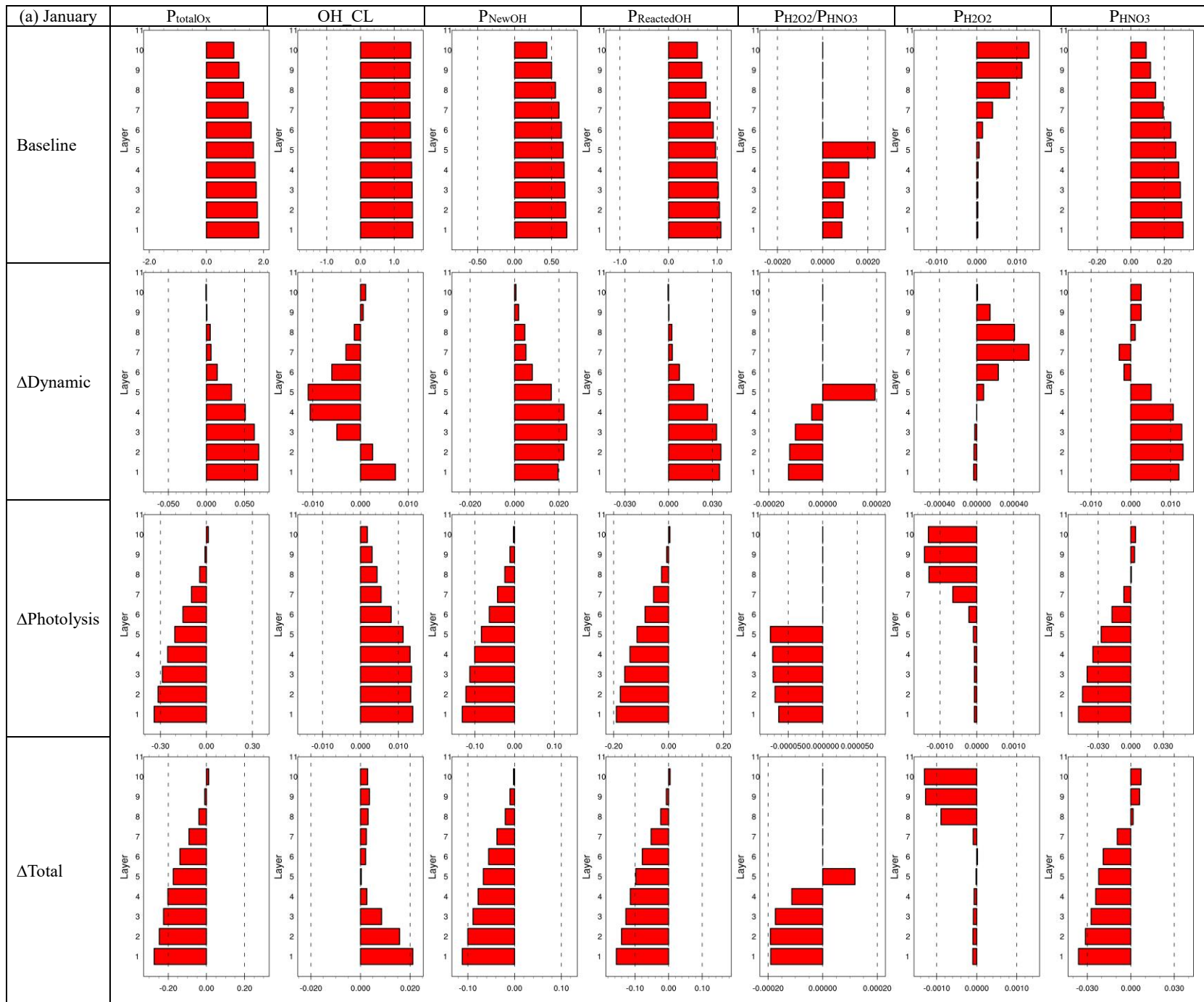


Figure 7: Impacts of ADE on surface O_x and OH (monthly average of noon time 11am-1pm local time)



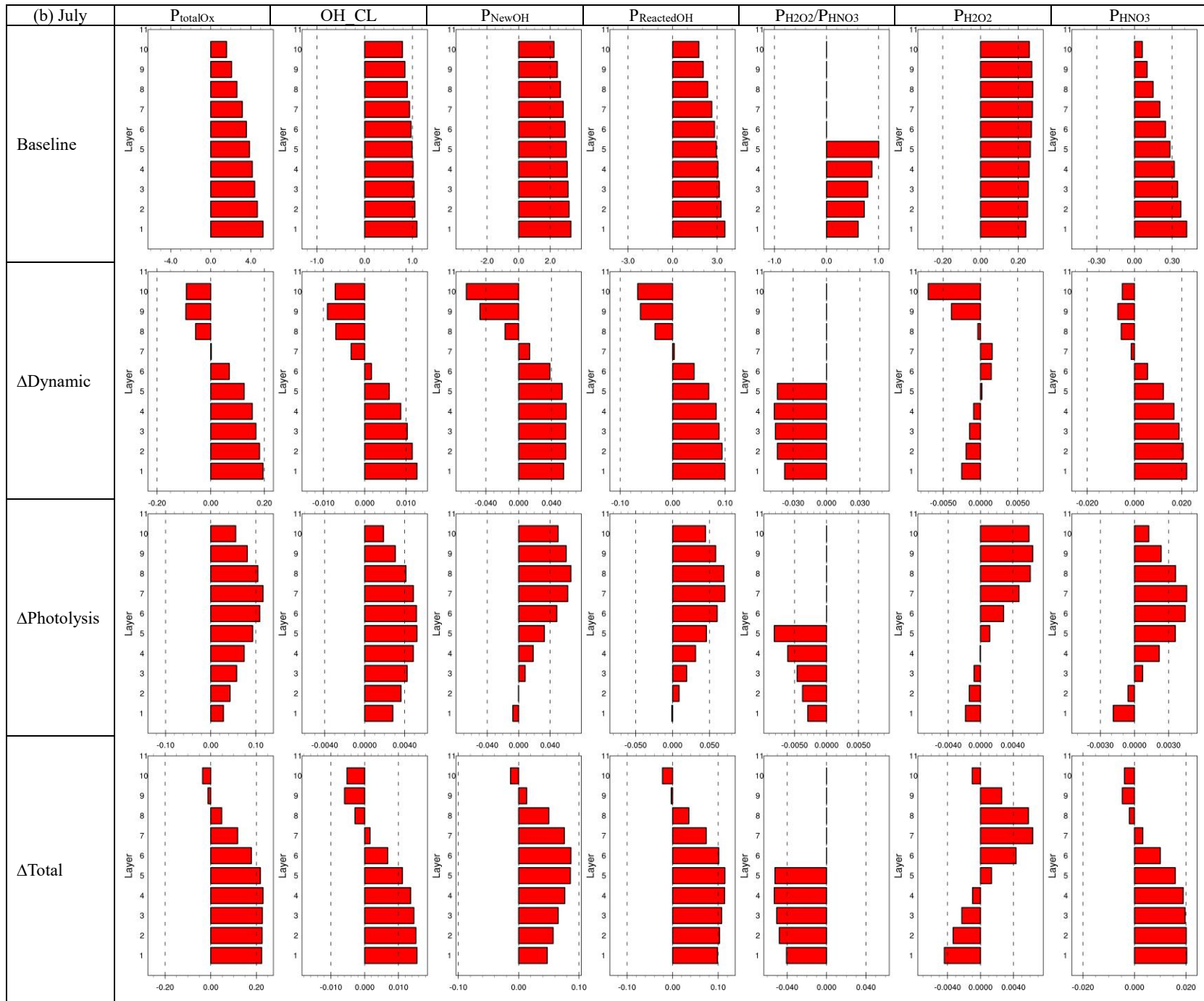


Figure 8: Vertical profile of integrated reaction rates in JJJ at noon (full-layer heights above ground are 40, 96, 160, 241, 355, 503, 688, 884, 1100, 1357m; Baseline is the simulation in SimBL; Δ Dynamic is the difference between SimSF and SimNF; Δ Photolysis is the difference between SimNF and SimBL; Δ Total is the difference between SimSF and SimBL; P_{totalO_x} is total O_x production rate, unit: ppb hr^{-1} ; OH CL is OH chain length; P_{NewOH} is the production rate of new OH, unit: ppb hr^{-1} ; $P_{\text{ReactedOH}}$ is the production rate of reacted OH, unit: ppb hr^{-1} ; $P_{\text{H}_2\text{O}_2}$ is the production rate of H_2O_2 , unit: ppb hr^{-1} ; P_{HNO_3} is the production rate of HNO_3 , unit: ppb hr^{-1} ; the ratio of $P_{\text{H}_2\text{O}_2}/P_{\text{HNO}_3}$ is only shown for layer 1-5)